H-mode grade confinement in L-mode edge plasmas at negative triangularity on DIII-D

A. Marinoni[1], M.E. Austin[2], A.W. Hyatt[3], M.L. Walker[3], J.Candy[3], C. Chrystal[3], C.J. Lasnier[4], G.R. McKee[5], T. Odstrčil[1], C.C. Petty[3], M. Porkolab[1], J.C. Rost[1], O. Sauter[6], S.P. Smith[1], G.M. Staebler[1], C. Sung[7], K.E. Thome[1], A.D. Turnbull[1], L. Zeng[7] and the DIII-D Team[1]

[1] *Plasma Science and Fusion Center, Massachusetts Institute of Technology, Cambridge (MA) USA*

[2] *University of Texas at Austin, Austin (TX) USA*

[3] *General Atomics, San Diego (CA) USA*

[4] *Lawrence Livermore National Laboratory, Livermore (CA) USA*

[5] *University of Wisconsin, Madison (WI) USA*

[6] *Swiss Plasma Center, Ecole Polytechnique Fédérale de Lausanne, Lausanne (VD) Switzerland*

[7] *University of California at Los Angeles, Los Angeles (CA) USA*

Plasmas with negative triangularity shape have been created on the DIII-D tokamak that, despite maintaining standard L-mode edge radial profiles, reach volume averaged pressure levels typical of H-mode scenarios. Within the auxiliary power available for this experiments, plasmas exhibit near zero power degradation sustaining $\beta_N = 2.7$ and $H_{98,y2} = 1.2$ for several energy confinement times. Detailed comparison with matched discharges at positive triangularity indicates that Trapped Electron Modes are weakened at negative triangularity, consistent with increased confinement and reduced intensity of electron density, electron temperature and ion density fluctuations. These results indicate that a negative triangularity plasma operating without an edge pedestal might provide an attractive scenario for operations in future reactors.

H-mode grade confinement in L-mode edge plasmas at negative triangularity on DIII-D

I.   INTRODUCTION

An economically viable fusion reactor will require a steady state scenario of operation able to sustain high pressure and energy confinement while maintaining the plasma relatively free of impurities to maximize the Lawson thereoftriple product; in the case of tokamaks, a substantial amount of stationary current will also have to be generated by either the plasma itself or external driving methods. The MHD theory defines limits to the pressure and current levels a given plasma can sustain, beyond which instabilities cripple or even zero performance, respectively, in the case of minor or major events. Restricting our attention to the research line of tokamaks, in the early '80 much research effort was devoted by the community to understand the maximum pressure achievable in tokamaks; Troyon derived a limit in simple form that closely matched that measured in existing machines[1] and generated real concern in the community because, if true, its low value would have hardly allowed opearion in a reactor. It was later realized that plasma shaping, which in the Miller formalism is commonly characterized by mainly two parameters named elongation (κ) and triangularity (δ), can strongly affect the Troyon limit. In particular, it was found that the stability limit in elongated plasmas exceeds that predicted by the Troyon limit thanks to the increased maximum current, at fixed edge safety factor, which in turn increases the maximum achievable pressure normalized to that of the confining magnetic field, or β[2,3]. Subsequent studies tackled the task of optimizing plasma triangularity; in particular it was found that large and positive values allow one to maximize the pedestal height of H-mode regimes[4,5], and thus increase confinement. In parallel to the stability analysis, the impact of shaping on turbulence was, at first, investigated mainly through linear Gyro-Fluid (GF) and Gyro-Kinetic (GK) simulations, whmarinoni triangularity ich focused on the effect of elongation on Ion Temperature Gradient (ITG) driven[6?] and Trapped Electron (TEM) modes[7]. Later studies confirmed the stabilizing effect of elongation on ITG and mixed ITG/TEM modes also in the non-linear regime both with local, or flux tubes, simulations[8,9] as well as with global modeling[10]. The impact of triangularity on turbulence was found by GK modeling to be negligible, at least compared to the effect of elongation, in the case of ITG dominated plasmas. It must be pointed out, however, that most of those studies were restricted to positive triangularity values, most likely due to the fact that ballooning modes are predicted to be more virulent at negative triangularity. Nevertheless, it was predicted in the early eighties

that negative triangularity has a stabilizing effect on TEM turbulence[7], although the effect was predicted to be smaller than that exerted by elongation. In the mid two-thousands experiments from the TCV tokamak showed that, in collision-less inner-wall limited plasmas dominated by TEM turbulence, the confinement time could by doubled simply by reversing triangularity with other parameters held fixed[11]. Those results, although in experimentally demonstrating the stabilizing effect of negative triangularity on TEM, were obtained in a regime of low pressure and pure electron heating for which the electron temperature was much higher than that of ions'. This motivated the experiments on the DIII-D tokamak presented in this work, which extends the TCV experiments to a more reactor relevant regime and higher β and where $T_e \simeq T_i$. The paper is organized as follows. Section II explains how the experiments were performed; Section III reports on low heating ($P_{aux} < 6$ MW) phases, during which matched discharges at negative and positive triangularity in L-mode phase are compared in terms of transport properties, intensity of fluctuations and gyro-kinetic modeling; Section IV describes the high heating phase, during which L-mode edge negative triangularity plasmas reach H-mode grade confinement; conclusions and perspectives are offered at the end.

II.   OVERVIEW OF DIII-D EXPERIMENTS

As it was mentioned in the introduction, the experiments were carried out on the DIII-D tokamak[12] to validate and extend earlier results obtained on TCV tokamak[13]; as such, some of the decisions made during the design of the experiment were dictated by the need to connect with the TCV plasmas analyzed in[11]: primarily, the plasma shape was chosen to be up-down symmetric. Since the DIII-D tokamak was not designed to realize unconventional plasma shapes such as those at negative triangularity, some of the shaping parameters and the plasma positioning in the vacuum vessel could not be chosen arbitrarily: e.g. elongation was kept fixed at $\kappa = 1.33$ and the Last Closed Flux Surface (LCFS) on the outboard midplane had to be positioned at R=2.18 m because of the location of the poloidal field coils F7A-F7B. The location of the separatrix on the outboard midplane is about 10 cm on the high field side of the position commonly used for DIII-D discharges and cannot be reached by the reciprocating Langmuir probe, reason for which measurements of the heat flux width in the near Scrape-Off Layer (SOL) were not possible. The choice of an up-down symmetric

H-mode grade confinement in L-mode edge plasmas at negative triangularity on DIII-D

equilibrium resulted into plasmas limited on the inner-wall of the vacuum vessel, and maintained as such, because the DIII-D wall is not designed to withstand flux resulting from strike-points on the low field side; a control system was implemented to prevent the plasmas from inadvertently divert or rapidly quench the discharge in case X-points had appeared in the vacuum vessel. Two up-down symmetric equilibria at negative and positive triangularity ($\delta = \pm 0.4$) were developed to compare transport coefficients and fluctuation characteristics between the two values of triangularity. It was decided that the two plasma shapes would have the same form of the LCFS, when mirrored around their vertical central line, with matched values for major and minor radii, elongation and absolute value of triangularity; this resulted in differences in volume and toroidal flux within 8%. It was decided to evaluate the impact of triangularity on confinement and fluctuations by comparing sister discharges with matched shape, plasma current, toroidal field, gas puff and auxiliary power. This choice was dictated by the need to minimize the number of trial discharges needed to complete the experiment, and is indeed a much less discharge-demanding procedure than tweaking the actuators to try matching volume, safety factor and pressure profiles in an effort to eliminate their impact on transport coefficients; nevertheless, it is a legitimate choice when it comes to compare different operational regimes in a fusion device where the main parameters such as auxiliary power, plasma current and toroidal field are fixed. At matched mirrored shape, current and toroidal field, the edge safety factor in plasmas at positive triangularity is 15% higher, on average, than in their negative triangularity counterparts; no attempt was made to evaluate the impact of shape on confinement at fixed safety factor also in view of the fact that the q-profile does not enter scaling laws of global confinement at fixed plasma current and field. The safety factor on-axis was allowed to decrease below unity, which gives the opportunity to evaluate the impact of triangularity on saw-teeth: results of these measurements will be presented in a separate publication. Discharge parameters are summarized in Table I for the two shapes.

Two heating phases were considered: an ECH-only and a mixed ECH-NBI phase: the former included sporadic torque balanced beam blips to allow the measurement of ion pressure and velocity profiles, and was used to study electron dominated regimes to connect with TCV results; the latter, which explored regimes where the ion temperature is close to that of electrons, featured ECH throughout to avoid ion heating dominated regimes which are not relevant to reactors. The EC power deposition, calculated with the linear ray-tracing code

H-mode grade confinement in L-mode edge plasmas at negative triangularity on DIII-D

	$^-\delta$	$^+\delta$
$I_p[MA]$	0.9	0.9
$B_T[T]$	2.0	2.0
$l_i[H]$	1-1.3	1-1.3
q_{lim}	4.2	5.3
$\langle n_e \rangle [m^{-3}]$	3-5	3-5
$P_{ECH}[MW]$	2-3	2-3
$P_{NBI}[MW]$	0-10	0-10
$a[m]$	0.59	0.59
$R_0[m]$	1.60	1.60
$V[m^3]$	13.9	13.1
κ_{LCFS}	1.33	1.33
δ_{LCFS}	-0.4	+0.4

TABLE I. Overview of parameters for the negative ($^-\delta$) and the positive ($^+\delta$) triangularity configurations: plasma current (I_p), vacuum toroidal magnetic field (B_T), internal inductance (l_i), safety factor at the limited flux surface (q_{lim}), line averaged electron density ($\langle n_e \rangle$), ECH and NBI auxiliary power ($P_{ECH} - P_{NBI}$), minor radius (a), major radius (R_0), volume (V), elongation and triangularity values at the separatrix (κ_{LCFS}, δ_{LCFS})

TORAY-GA[14], is strongly radially localized slightly outside the $q = 1$ surface to minimize sawtooth activity. For the explored line averaged densities, ranging from $3 - 5 \cdot 10^{19} m^{-3}$, the EC power absorbed in the first pass through the EC resonance is typically larger than 98.5%, with current drive negligibly within 2 kA. The poloidal injection angle had to be adjusted for the two values of triangularity to guarantee the deposition of EC power at the same location in plasma coordinates. Real-time controlled gas puffing was generally used to control the line averaged density. The electron temperature was measured by the Thomson Scattering (TS) as well as by the Electron Cyclotron Emission (ECE) diagnostics; density was gauged by TS, CO2 Interferometer and microwave reflectometry; ion temperature along with toroidal and poloidal velocities were obtained by the Charge Exchange Recombination diagnostic (CER); fluctuations were monitored by the Phase Contrast Imaging diagnostic[15], the Beam Emission Spectroscopy (BES)[16] along with the Correlation Electron Cyclotron Emission

H-mode grade confinement in L-mode edge plasmas at negative triangularity on DIII-D

(CECE)[17]. The normalized radial coordinate used throughout this paper is defined as the squared root of the normalized toroidal flux.

III. EFFECT OF TRIANGULARITY ON CONFINEMENT AND FLUCTUATIONS

A. Effect on confinement

In this section we evaluate the impact of triangularity on confinement and fluctuations by comparing two discharges at opposite values of edge triangularity ($\delta_{LCFS} = 0.4$ and $\delta_{LCFS} = +0.4$) that have matched actuators throughout the entire shot length. Two heating phases are evaluated: pure electron heating achieved with ECH, and mixed ion-electron heating through combined ECH-NBI. The line-average density is maintained the same between the two shapes in the ECH-only heating phase, while it tends to differ when the NBI system is used. Both discharges operate with an L-mode edge and are thus free of ELMs. It is worth mentioning that, since about 35% of the NBI power couples to electrons, even during the combined ECH-NBI heating phase the plasmas are in an electron-flux dominated regime, despite the fact that the auxiliary power coupled by the NBI system is approximately equal to that from the EC system. In the discharges analyzed in this section, MHD activity is either limited or absent. Kinetic equilibria were reconstructed using the ONETWO transport code and the EFIT equilibrium solver which, by highly weighting constraints on core measurements from the Motional Stark Effect (MSE) diagnostic, was forced to recover a solution for which the electron temperature profiles from the ECE High-Field-Side and Low-Field-Side systems overlap, thereby ameliorating the accuracy on magnetic axis position. In order to estimate confidence intervals on the resulting heat diffusivities, series of one hundred simulations per discharge and time slice were carried out with the ONETWO transport code, with random variations of kinetic profiles, radiated power and wall recycling within their experimental uncertainties. The volume integrated radiated power is less than 25% of the total heating power and is typically equal for the two shapes within experimental uncertainties. In figure 1a, where we display kinetic profiles during the ECH-only phase, it can be seen that both discharges feature closely matched electron density, ion temperature and toroidal velocity profiles, while the electron temperature is up to 20% higher for the

6

H-mode grade confinement in L-mode edge plasmas at negative triangularity on DIII-D

discharge at $\delta_{LCFS} = 0.4$, although non uniformly across the radial profile. A reconstruction of the kinetic equilibrium shows that, by merely reversing edge triangularity, the plasma stored energy content increases by about 25%. The resulting electron heat diffusivities decrease by 20% to 80% in the region outside the ECH deposition location, with the difference increasing monotonically with the minor radius; in contrast, the ion heat diffusivity is much less sensitive to shape as, although systematically, it is lower at negative triangularity by less than one population uncertainty, σ (Fig.2). In the combined EC-NBI heating phase, with plasma profiles shown in figure 1b, we observe variations in all kinetic profiles: as compared to the discharge at $\delta_{LCFS} = +0.4$, the negative tringularity case features a 20% increase for on-axis electron density with about the same edge value, while T_e, T_i and Ω_ϕ are higher in the radial region $0.4 < \rho < 0.9$, with cross-overs on axis and at the edge. A kinetic analysis shows that, even in this regime where $T_e \simeq T_i$, the effect of reversing triangularity causes the stored energy to increase by 20%, while electron heat diffusivities decrease by 25-30% in the radial region $0.4 < \rho < 0.9$, with larger differences computed at outer radii, and the deuterium heat diffusivity being lower in the region $0.5 < \rho < 0.9$, although within one population uncertainty σ (Fig.2). It is important to mention that, for both heating schemes, the effective mid-radius inverse effective collisionality, defined as the electron collision frequency normalized to the bounce time, was typically less than two. This might partly explain why the confinement improvement at negative triangularity is observed to be significantly lower than that in the TCV experiments, where the effective collisionality was lower by a factor of two to three as compared to the DIII-D experiments reported in this work. Technical issues probbaly related to error field correction did not allow us to explore plasmas at lower density, which is a study deferred to future experiments.

B. Effect on the measured intensity of fluctuations

The intensity of electron density fluctuations was monitored by the Phase Contrast Imaging diagnostic that images line-integrated density fluctuations onto a linear array of 32 element detectors. The vertical line of sight, shown in figure 3, has its centerpoint located at $R = 1.98m$, which corresponds to the laser beam line being tangent to the flux surfaces roughly around mid-radius. The gaussian full-width at $1/e$ points in electric field is 7 cm which, together with the minimum aperture stop in the optical system, set the detectable

H-mode grade confinement in L-mode edge plasmas at negative triangularity on DIII-D

wave-number range to 1.5 to 35 cm^{-1}. The linear array is such that the diagnostic can reconstruct wavelets in the range $k_R < 25cm^{-1}$, and in the frequency range $10kHz < f < 2MHz$, with the lower cut-off set by a high-pass filter aimed at reducing the impact of mechanical vibrations on the measurements[15]. Since the systems performs a line integral of density fluctuations along a vertical direction in the laboratory frame, it is sensitive to scattering wavelets propagating in the horizontal plane; this translates into measured wave-vectors having varying poloidal and radial components in the plasma frame along the line of sight. In both heating phases, as shown in figure 4a, the intensity of density fluctuations is seen to decrease at all $f > 20 - 30kHz$ at negative triangularity. A quantitative comparison of the rms values shows that the total intensity of fluctuations, normalized to the line-averaged density along the PCI line of sight, decreases by 40% and 30%, respectively, in the EC-only and EC-NBI heating phases.

Wavenumber spectra displayed in Fig.4b indicate that the frequency integrated intensity of fluctuations at positive and at negative wave-vectors are different in the two shapes. More specifically, while at positive triangularity the wave-number spectra are roughly symmetric, at negative triangularity the total power at positive wave-vectors is lower than that in the negative part of the spectrum. Since both configurations are up-down symmetric and this imbalance is observed even in the ECH-only phases during which flow shear is low, this feature suggests that turbulent eddies might be oriented in different ways in the two shapes, which would be consistent with exploratory linear simulations with the LORB5 code[11], which showed that profile shearing effects are more prominent at negative triangularity and induce a poloidal tilt to turbulent eddies, resulting in larger $k_\perp$ and reduced mixing-length diffusivities. The asymmetry in the PCI response is due to the line integral, which strongly weights turbulent eddies aligned orthogonally to the laser beam direction of propagation, while it averages out eddies aligned along it. This mechanism is equivalent to asymmetries detected in flow-sheared plasmas: low-shear regimes, such as L-mode, typically create spectra symmetric in k_R, while highly-sheared H-mode edge typically create asymmetric wave-number spectra[18]. Ion density fluctuations were monitored by the Beam Emission Spectroscopy (BES) diagnostic, which is sensitive to wave-vectors in the range $k_\perp < 2cm-1$ at frequencies less than 1 MHz[16]. The diagnostic measures density of fluctuations on a radially movable array of 64 elements, which for the present experiments were disposed in a poloidal-radial configuration of an 8x8 matrix. As it is shown in Fig.5a, where

H-mode grade confinement in L-mode edge plasmas at negative triangularity on DIII-D

fluctuations data from two repeat discharges at positive triangularity offer a wide coverage in minor radius, the intensity of fluctuations in the combined NBI-ECH heating phase to decrease at negative triangularity by an amount typically larger than errorbars. It is interesting to report that the absolute reduction of the relative intensity of fluctuations is an increasing function of the minor radius, which approximately follows the radial penetration length of triangularity. Electron temperature fluctuations were monitored with the Correlation Electron Cyclotron Emission system (CECE), which simultaneously samples eight locations along a radial line of sight 7.6 cm above the plasma mid-plane[17]. The system samples fluctuations in the frequency range $f < 1MHz$, is sensitive to wave-vectors $k < 2cm^{-1}$ and has a floor noise of approximately 0.3% when sampling data for one second length. In both heating regimes, the relative intensity of fluctuations is seen to decrease at negative triangularity by approximately 10-15%. It is important to underline that, as opposed to the BES diagnostic, the observed reduction does not seem to depend on the radial location, at least in relative terms, as displayed in Fig.5b. It is an open question whether such behavior, recently observed also on TCV with a CECE and a PCI system[19,20] is due to global effects[21,22]. Detailed non-linear gyro-kinetic simulations are deemed necessary to interpret the above observations through synthetic diagnostics.

C.   Linear gyro-kinetic modeling

Early non-linear local gyro-kinetic simulation of TCV discharges found that the increased confinement at negative triangularity was due to a weakening of Trapped Electron Modes, which were the dominant instability in those cases, caused by a modification of the toroidal precession drift exerted by negative triangularity[21]. The CGYRO code[23] was used to evaluate the linear modes at play in these discharges. Simulations were executed by obtaining kinetic equilibria reconstructed with the EFIT equilibrium code and subsequently read directly by CGYRO. Eigenvalues were modified by less than 10% when using a Miller parametrization of the equilibrium, which suggests that the numerical equilibrium is correctly evaluated by CGYRO even in this unusual shape. In both heating regimes and across the minor radius, TEM are found to be the dominant instability in the wave-number region $0.3 < k_\theta \rho_s < 1$, consistent with the discharges being in an electron-flux dominated regime. Sensitivity studies show that TEM in these plasmas respond almost equally to the same relative perturbation

H-mode grade confinement in L-mode edge plasmas at negative triangularity on DIII-D

in the electron temperature and in the electron density scale lengths. By artificially reducing collisionality, TEM are predicted to become more virulent, as expected, while the difference in growth-rates between the two shapes slightly increases. At electron scales ETG modes are predicted to be unstable at all radii and heating phases. Depending on radius, heating phase and profiles uncertainties, Ion Temperature Gradient (ITG) modes are seen at times become the dominant instability at the low-end of the wavenumber spectrum. Linear simulations carried out with the same plasma profiles on the two equilibria at opposite values of triangularity indicates that, as expected from previous work described in earlier sections, growth rates are reduced at negative triangularity in the TEM dominated region while ETGs are almost insensitive to the shape change. A survey of growth-rates was done on actual profiles along with ten random variations thereof within experimental uncertainties; although the stabilization at ion scales exerted by negative triangularity is robust accross radius and heating phases, the reduction in growth-rates is an involved function of radius, wavenumber and heating phase and reflects the complex radial structure of the measured inverse scale lengths and ion to electron temperature ratios. In particular, as it can be seen in Fig.6, even though the reduction in the linear growth rates is usually larger than the population errorbar associated with profile uncertainties, it is not rare to find subregions in radius and wavenumber space in which differences in growth rates are within uncertainties. Since the trapped particle fraction increases at negative triangularity, it cannot explain the stabilizing effect on TEM and the confinement increase. During both heating phases, growth-rates at electron scales are modeled to decrease at all radii in the negative triangularity equilibrium due to a reduced inverse electron temperature scale length. Indeed, consistent with observations reported in[24], in the plasma region $\rho > 0.9$, the electron temperature radial profile is seen to increase more rapidly at negative triangularity, while similar gradients are measured in the region $0.5 < \rho < 0.9$; this feature creates a sort of pedestal, although much lower than an actual H-mode pedestal, that makes the inverse electron scale length lower at negative triangularity. The difference in the edge gradient between the two shapes is postulated in[24] to be due to a larger critical gradient for the onset of electron-scale fluctuations at the very edge of negative triangularity plasmas, which would be consistent with non-linear flux-tube gyro-kinetic simulations reported in[22]. The predicted presence of strong ETG modes in the plasmas described in this report constitutes a major difference with respect to the TCV experiments, in which such modes were stable everywhere inside $\rho \simeq 0.9$ partly due to the

H-mode grade confinement in L-mode edge plasmas at negative triangularity on DIII-D

much higher T_e/T_i ratio.

IV. HIGH HEATING PHASE AND H-MODE CONFINEMENT WITH L-MODE EDGE

The high heating phase of these experiments was obtained mainly through ion heating, up to an administrative limit of 12 MW, including $2-3$ MW of EC heating deposited slightly inside mid-radius.

An intriguing observation of this experiment is that, even for discharges at matched density and actuators, the LH power threshold appears to be significantly higher at negative triangularity. Indeed, while plasmas at positive triangularity usually exhibit a regular transition to a limited H-mode phase when the auxiliary power exceeds $6-7$ MW, no LH transition in plasmas at negative triangularity was observed within the administrative power limit and, consequently, all plasmas at negative triangularity described hereafter maintain edge pressure profiles typical of an L-mode phase. The higher LH power threshold does not appear to be due to a difference in the power flux passing through the separatrix, nor to an imbalance between ion and electron energy fluxes between the two shapes. Although the two equilibria are no longer comparable in terms of diffusivities and fluctuations because they are in two distinct confinement regimes, especially near the edge where plasmas at positive triangularity feature a regular H-mode pedestal, it is still legitimate to compare their global, or volume integrated, properties. In figure 9 we display a comparison of two pairs of sister shots at matched actuators, for which the discharges at positive triangularity transition to H-mode. It is remarkable to note that discharges at negative triangularity, despite maintaining edge pressure profiles typical of an L-mode phase that do not trigger any ELM, reach global confinement values quantitatively comparable to those featured by the sister discharges at positive triangularity reaching pressure and confinement values typically observed in H-mode plasmas. These discharges reach $\beta_N > 2.5$, confinement factor, $H_{98y,2} > 1$ and, at least on the DIII-D tokamak, set a record for L-mode discharges at full field. The H-mode grade confinement level obtained in L-mode edge plasmas at negative triangularity is particularly apparent when visualizing the functional dependence of stored energy on the coupled power computed by the ONETWO code, which uses TORAY-GA and NUBEAM for ECH and NBI, respectively. As shown in figure 7, where such dependence is

compared to that from the H89P[25] power scaling law computed at the experimental value of line averaged density, plasma current and toroidal field, the stored energy in negative triangularity plasmas progressively exceed that of the scaling law, barely reaching a factor of two increase at the highest power, which corresponds to a rough definition of H-mode in terms of pure global confinement values. Studies at low or zero auxiliary torque were not possible in this experiment due to time constraints and are deferred to future experiments. The H-mode level pressures sustained by these negative triangularity discharges are constantly reached in the high heating phase, regardless of the heating trajectory, as it can be understood by looking at figure 9, and were not limited by stability.

Indeed, as it can be seen in Figure 8, the high pressure phase can be sustained for several energy confinement times without any ELM event. Additionally, the normalized pressure constantly raises following a power staircase increase without any sign of saturation or collapse, which indicates that the achieved values for normalized pressure is not due to plasma stability, rather to the administrative power limit imposed on these experiments. The ideal β limit for this up-down symmetric shape at negative triangularity was estimated to be approximately three by using a procedure developed in[28]. A number of kinetic equilibria corresponding to various times of one of the negative triangularity discharges was first reconstructed with the equilibrium code EFIT. Since sawtooth oscillations are generally active in these plasmas, the β limit for the onset of an internal pressure driven kink mode is evaluated by estimating, as a function of pressure, a threshold in β_N above which growth rates and edge displacement increase sharply. Such threshold is compared to the onset of an $n = 1$ mode in a modified equilibrium in which the safety factor is artificially raised above unity to avoid the sawtooth oscillation: ideally, the two $beta_N$ limits should approximately coincide. The equilibrium from EFIT was read by the equilibrium code CORSICA[29] that was used to compute an inverse equilibrium after a slight modification of the q-profile to make it larger than unity at revery radius. Subsequently, various equilibria corresponding to a pressure scan were genrated by CORSICA and evaluated by the stability codes GATO[26] and DCON[27]. In figure 10a we display an example of the $beta_N$ dependence of growth rates for an $n = 1$ mode predicted by GATO for the original, or sawtoothing, equilibrium and a modified equilibrium.

It is interesting to note that, as shown in figure 10b, the beta dependence of the growth-rates features a break in slope across the predicted β limit, which shows that the sawtooth and the

H-mode grade confinement in L-mode edge plasmas at negative triangularity on DIII-D

internal pressure driven kink have different concavity values as functions of β_N. Sensitivity studies on the effect of the modified q-profile on the estimated β limit were carried out by varying the minimum of the modified q-profile, its radial location, and the flux surface at which the modified safety factor merges with the original profile smoothly up to the second radial derivative, all of which are arbitrary parameters. Pressure scans were carried out on forty different time instants and twenty modified q-profiles per time slice with the DCON code, resulting in a 7% relative change in the estimated β limit; the reason for such low sensitivity is likely due to the relatively flat pressure gradient that resides in the regions where the safety factor was modified.

The comparison of high pressure plasmas at negative triangularity with an L-mode edge and actual H-mode plasmas at positive triangularity can be taken a step forward and evaluate bootstrap current and neutron yield. While it is generally true that the pedestal region provides a large fraction of the total bootstrap current, due to the combined effect of large pressure gradients and the large area enclosed by flux surfaces near the LCFS, inner regions can significantly contribute, especially if large pressure gradients are sustained over a significant fraction of the minor radius. This is particularly apparent in figure **??**, where we compare the radial profile of the bootstrap current density for the two sister discharges displayed in Fig.9a at 2.2 s. While the positive triangularity plasmas features an H-mode pedestal, as evidenced by the large peak in the current density near the LCFS, the plasma at negative triangularity maintains an L-mode edge and is therefore free of the edge current peak. However, thanks to the larger pressure gradients developed across the minor radius allowed by lower anomalous transport at fixed heating power, inner regions at negative triangularity contribute up to 50% more than at positive triangularity, resulting in the negative triangularity plasma generating 18% more bootstrap current that its positive triangularity counterpart. The pair of discharges from Fig.9b, for which H-mode pedestal is steeper and offers 15% increase in β_N compared to the sister discharge at negative triangularity, results in 23% more bootstrap current produced at positive triangularity as computed by the NEO code. The difference in the bootstrap current at inner radii is not due to the trapped particle fraction because this quantity can be shown to be identical for the two shapes within 8% at the LCFS, which is where the largest difference takes place.

The neutron rate in high confinement L-mode edge plasmas at negative triangularity is measured to be 30-60% higher than that in H-mode plasmas at positive triangularity at

H-mode grade confinement in L-mode edge plasmas at negative triangularity on DIII-D

matched values of plasma current, toroidal field, line averaged density and auxiliary power. Figure **??**, where we display the time evolution of relevant quantities for the two shapes, suggests that the reason for the increased neutron rate is main ion dilution caused by the higher effective charge displayed by the positive triangularity discharges when entering the H-mode phase. This is confirmed by time dependent simulations of the neutron rate carried out with the TRANSP code; as it can be seen in figure 12, the simulated neutron rate, which is close to the experimental value when the interpretative simulation is run on the actual experimental data for the two triangularities, can be almost reversed when the carbon content is swapped between the two equilibria. The much higher carbon content measured at positive triangularity is certainly partly due to the edge barrier that retains impurities, although we cannot exclude a larger carbon source from the wall. Indeed, as compared to negative triangularity plasmas that maintain an L-mode edge, the C^{III} line intensity from a DIII-D filterscope that looks at a location close to the inner-wall region used as a limiter in this experiment sharply decrease as plasmas enters the H-mode regime, but then quickly saturate due to the first few ELMs. Data on the C^{II} line are not available. The Laser Blow-Off system, that was recently installed on DIII-D, was used in follow-up experiments to estimate the impurity confinement time in high confinement plasmas at negative triangularity. The injected impurity was Aluminum because its charge exchange cross section data allow accurate analysis. The decay rate of the Al^{XIII} density was measured by the CER system to be 64 ms for a chord close to the magnetic axis, with lower values at outer radii, which is quantitatively similar to those extracted from previous measurements in regular L-mode plasmas. Although we were not able ti employ the LBO system in matched discharges at positive triangularity, the imurity confinement time in H-mode plasmas on DIII-D has consistently been measured to be longer than 160 ms[30]. The ratio of the particle to the energy confinement times, τ_P/τ_E, is of order unity for these plasmas while it is usually larger by a factor of 2-3 in H-mode plasmas[?] . These data show that high pressure plasmas at negative triangularity, by maintaining edge pressure profiles typical of L-mode phases, offer high energy and low impurity confinement, which is a desirable property for a fusion reactor.

V. CONCLUSIONS

Inner-wall limited discharges at negative triangularity have been created on the DIII-D tokamak and compared to discharges with the same shape of the LCFS, but at positive triangularity, at matched values of plasma current, confining magnetic field and auxiliary power. In both pure electron heating (up to 3 MW of ECH) and combined electron-ion heating (up to 6 MW evenly divided between ECH and NBI), plasmas at negative triangularity feature increased confinement and lower heat diffusivities, primarily on the electron channel, accompanied by decreased intensity of fluctuations in electron density, ion density and electron temperature as measured by the Phase Contrast Imaging, The Beam Emission Spectroscopy and the Correlation Electron Cyclotron Emission diagnostics, respectively. The overall reduction of the intensity of fluctuations is in the range 10%-30% depending on the diagnostic, on the heating scheme as well as on the coupled power; this is in quantitative agreement with the increase in stored energy which is of the same order of magnitude. A linear gyro-kinetic analysis shows that plasmas, regardless of triangularity, are dominated at ion-scale by Trapped Electron Modes (TEM) in both heating schemes and across the minor radius, with Electron Temperature Gradient (ETG) modes destabilized at electron scales. Depending on the actual coupled power as well as on the radial location being analyzed, Ion Temperature Gradient (ITG) modes appear at times as the dominant instability in the low-end part of the wave-vector spectrum. Negative triangularity is seen to stabilize TEM at all radial locations examined; the amount of stabilization, which usually exceeds the impact of experimental uncertainties on growth rates, is not uniform in radius and wavenumber, due to plasma profiles being different in the two shapes. In the high heating power phase, where the NBI power was increased up to 9 MW while maintaining ECH power constant, plasmas show near zero power degradation and sustain, for several energy confinement times, volume averaged pressure levels typically observed in H-mode discharges. These plasmas reach $\beta_N = 2.7$ and $H_{98,y2} \simeq 2$, despite maintaining edge pressure profiles typical of L-mode plasmas and therefore naturally free of Edge Localized Modes (ELMs). The ideal β limit for these discharges is predicted by the GATO code to take place at $\beta_N \simeq 3$; such value would be suitable in a reactor provided that the L-mode edge can be maintained. High pressure plasmas in this shape offer low impurity retention compared regular H-mode plasmas for a comparable energy confinement.

H-mode grade confinement in L-mode edge plasmas at negative triangularity on DIII-D

VI. ACKNOWLEDGEMENTS

REFERENCES

[1] F. Troyon et al., Plasma Phys. Control. Fusion 26 (1984) 209

[2] T. Taylor et al., GA report 1994

[3] F. Hofmann et al., Phys. Rev. Lett. 81 (1998) 2918

[4] T.H. Osborne et al., Plasma Phys. Control. Fusion 42 (2000) A175

[5] P.B. Snyder et al., Nucl. Fusion 44 (2004) 320

[6] D.D. Hua et al., Phys. Fluids B 4 (1992) 3216 and R.L. Miller, Phys. Plasmas 6 (1999) 4265

[7] G.Rewoldt et al., Phys. Fluids 25 (1982) 480

[8] E. Belli et al., Phys. Plasmas 15 (2008) 092303

[9] J.E. Kinsey et al., Phys. Plasmas 14 (2007) 102306

[10] P. Angelino et al., Plasma Phys. Control. Fusion 48 (2006) 557

[11] Y. Camenen et al., Nucl. Fusion 47 (2007) 510

[12] J.L. Luxon, Nucl. Fusion 42 (2002) 614

[13] F. Hofmann et al., Fusion Technol. 1 (1986) 687

[14] A. H. Kritz et al., Conference Proceedings, 3rd Intl. Symp. on Heating in Toroidal Plasmas ECE, Brussels Vol. 2 (1982) 707

[15] J.R. Dorris et al., Rev. Sci. Instrum. 80 (2009) 023503

[16]G.R. Mckee et al., Rev. Sci. Instrum. 81 (2010) 10D741

[17]C. Sung et al., Rev. Sci. Instrum. 87 (2016) 11E123

[18]J.C. Rost et al., Phys. Plasmas 21 (2013) 062306

[19]M. Fontana et al., Nucl. Fusion 58 (2018) 024022

[20]Z. Huang et al., submitted to PPCF

[21]A. Marinoni et al., Plasma Phys. Controll. Fusion 51 (2009) 055016

[22]G. Merlo et al., Plasma Phys. Controll. Fusion 57 (2016) 054010

[23]J. Candy et al., Comput. Phys. Commun. 324 (2016) 73

[24]O. Sauter et al., Plasma Phys. Controll. Fusion (2014)

[25]P.N. Yushmanov et al., Nucl. Fusion 30 (1990) 1999

[26]L.C.Bernard et al., Comput. Physics Commun. 24 (1981) 377

[27]A.H. Glasser, Phys. Plasmas 23 (2016) 072505

[28]A.D. Turnbull et al., Fusion Science and Technology 48 (2005) 875

[29]J.A. Crotinger et al., LLNL Report UCRL-ID-126284 NTIS #PB2005-102154 (1997)

[30]T. Odstrčil, private communication

H-mode grade confinement in L-mode edge plasmas at negative triangularity on DIII-D
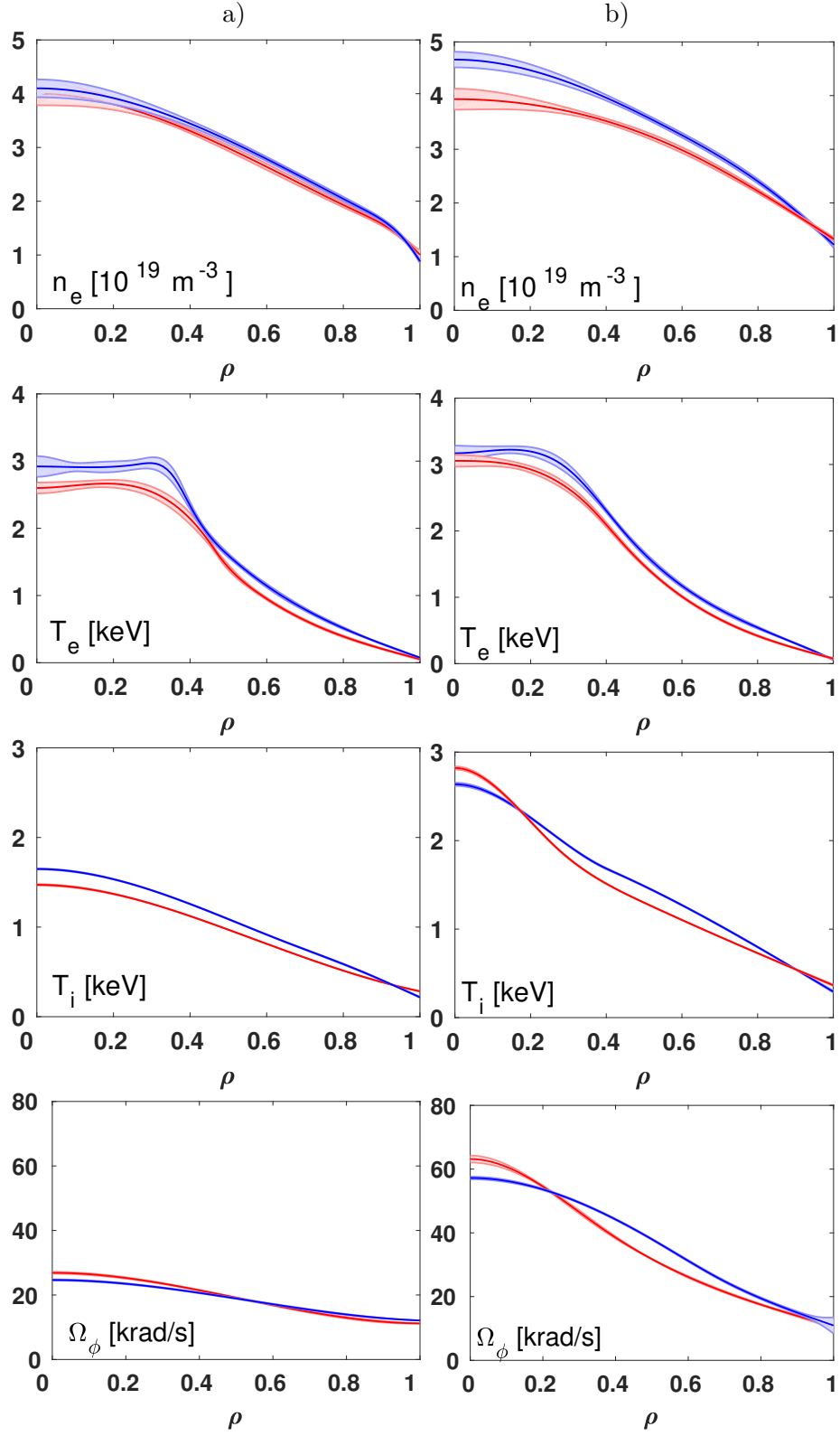
FIG. 1.   Snapshot of typical radial profiles of electron density, electron temperature, carbon temperature and carbon toroidal rotation frequency for the two equilibria at mirrored values of triangularity during ECH-only heating phase (a) and combined ECH-NBI phase (b).
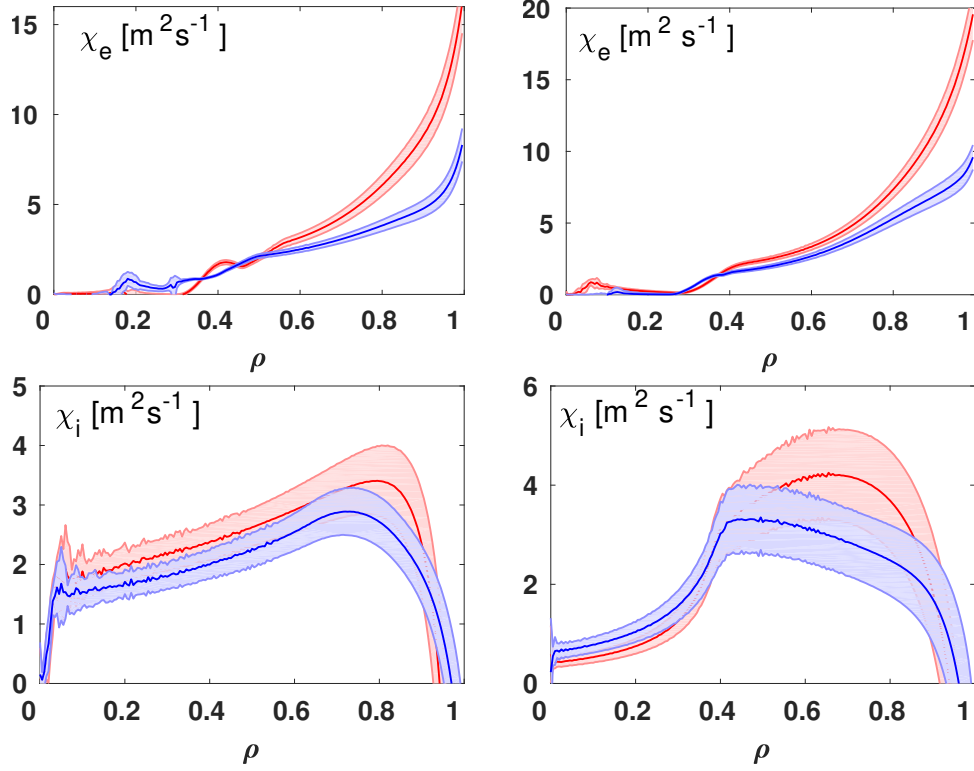
FIG. 2. Electron (top) and ion (bottom) heat diffusivities for the cases displayes in Fig.1a (left) and Fig.1b (right).

FIG. 3. Comparison of the cross sections of the two triangularity discharges along with the measurement locations, or line of sights, of the fluctuations diagnostics used in this work.
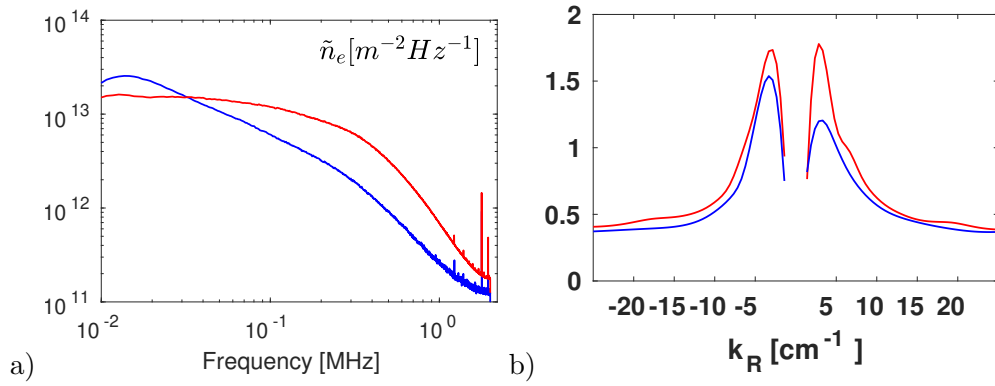
FIG. 4. (a) Frequency spectra of density fluctuations from the PCI diagnostic for the combined ECH-NBI heatng phase for the two triangularity cases. (b) Wave-number spectra.
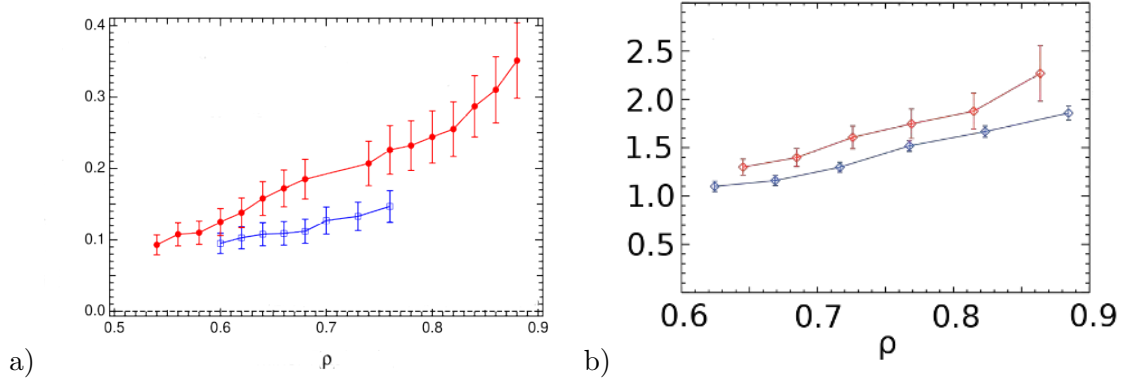
FIG. 5.   Radial dependence of the relative intensity ion density (a) and electron temperature (b) fluctuations measured by the BES and the CECE systems, rspectively.
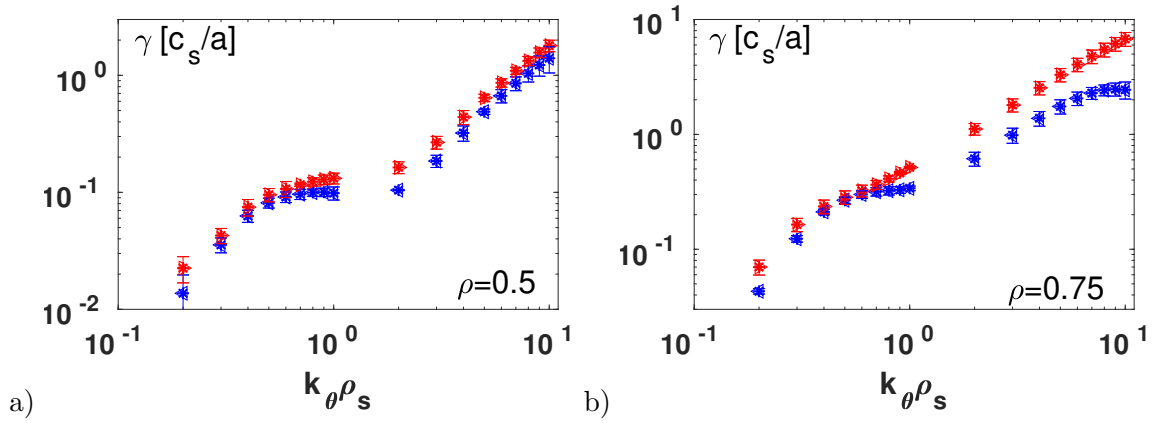
FIG. 6.   (a) Linear growth-rates computed by the CGYRO code on actual experimental profiles at $\rho = 0.5$ and in a time slice with a combined ECH-NBI heating for both values of triangularity. (b) Same as (a) but computed at $\rho = 0.75$.
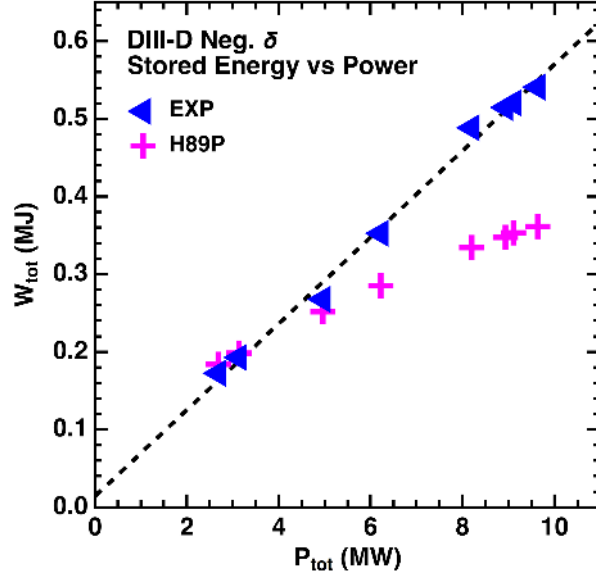
FIG. 7.   Dependence of stored energy on coupled power for a number of plasma discharges at negative triangularity (blue rectangles) compared to the H89P power scaling law computed at the corresponding values for plasma current, toroidal field and line averaged density.
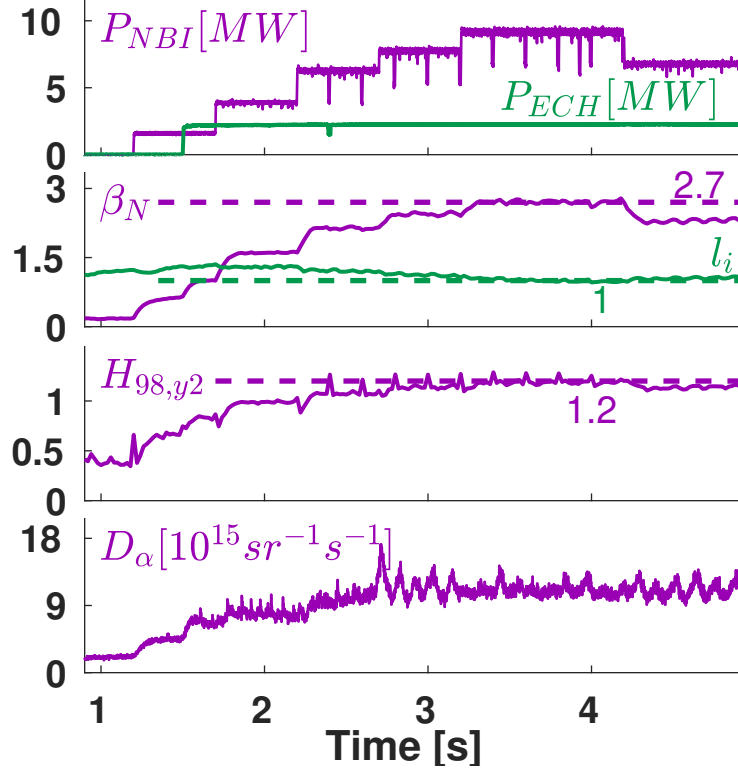
FIG. 8. From top to bottom, time histories of auxiliary power, β_N and internal inductance, $H_{98,y2}$ confinement enhancement factor, D_α signal from one of the filterscopes whose line of sight intersects the confined plasma in both shapes.
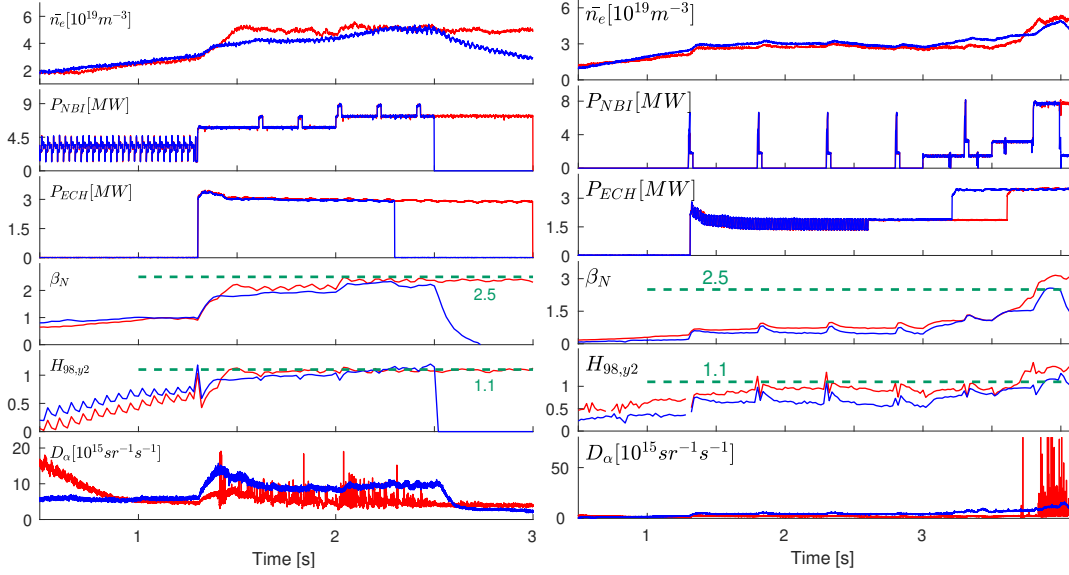
FIG. 9.   Comparison of two pairs of sister discharges at opposite values of triangularity and at matched values of plasma current, toroidal field and auxiliary power in terms of, from top to bottom, line averaged density, NBI power, ECH power, normalized pressure β_N, confinement factor $H_{98,y2}$, D_α signal.
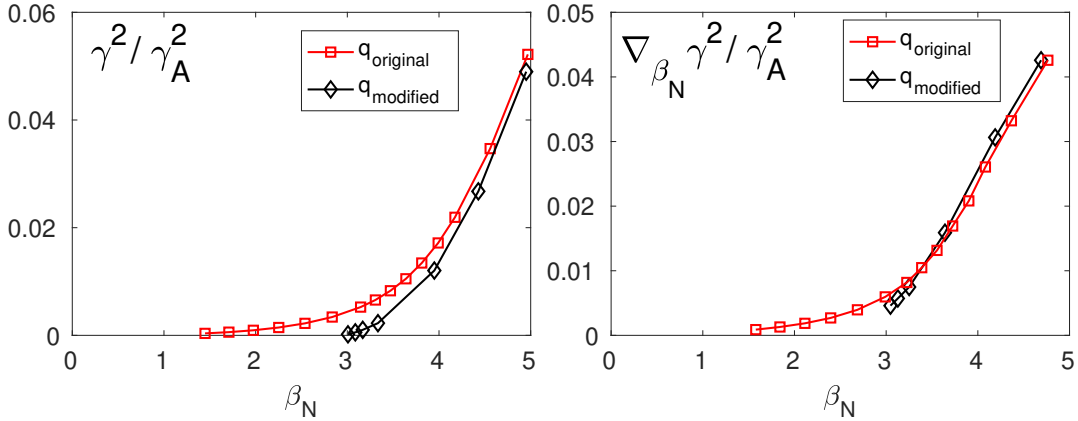
FIG. 10.   Pressure dependence of the growth-rates for an ideal $n = 1$ mode predicted by GATO (left) and their pressure gradient (b) for the original (red squares) and one of the modified q-profiles (black diamonds).
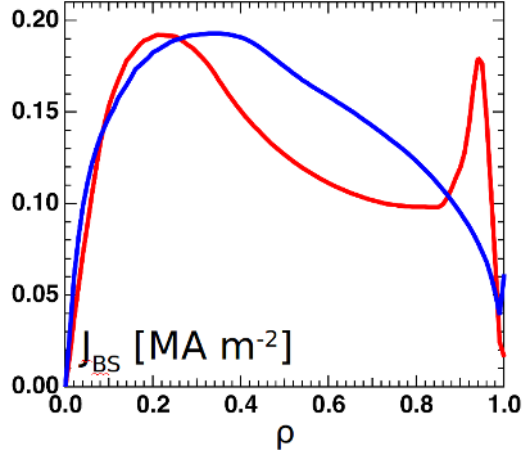
FIG. 11. Comparison of the radial profile of the bootstrap current density for discharges at positive (blue) and negative (red) triangularity shown in Fig.9a computed in a timeslice at 2.2 s
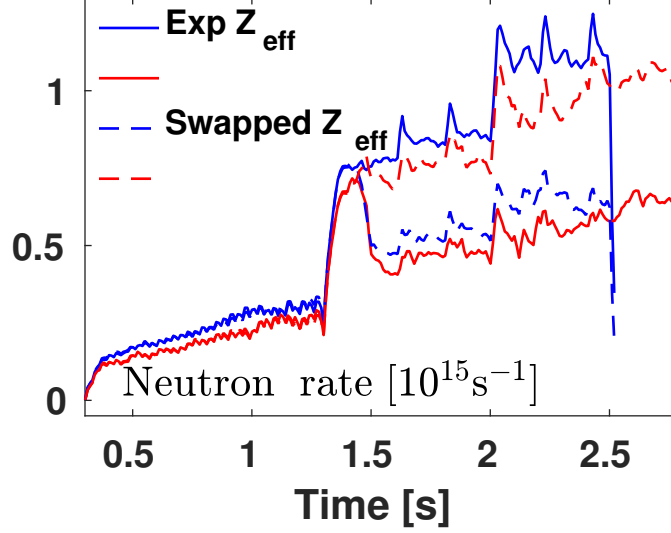

FIG. 12. Time evolution of the neutron rate predicted by the TRANSP code for two matched plasma discharges at positive (red) and negative (blue) triangularity. Simulations are carried out on actual experimental data (solid) and for a case in which the carbon content has been swapped between the two equilibria (dashed).
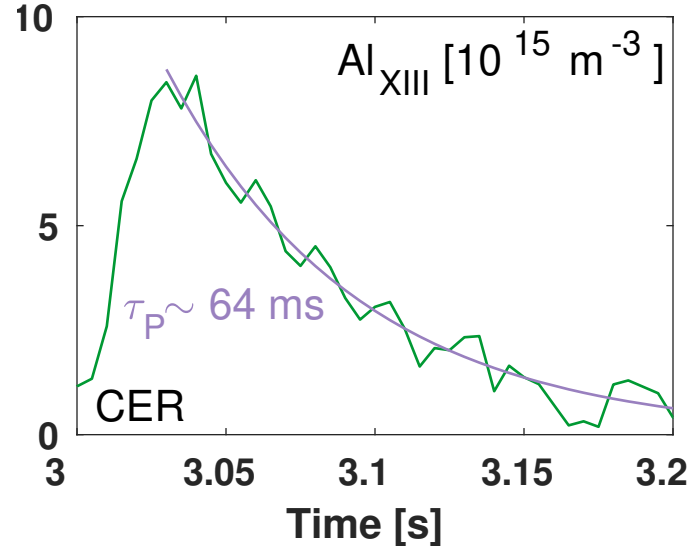
FIG. 13.   Time evolution of the Al density seen by a CER line of sight close to the magnetic axis in response to a laser blow-off ablation at 3.0 s, along with an exponential fit indicating the confinement time.